THE ASTROPHYSICAL JOURNAL, Vol. 155, February 1969

# COSMIC-RAY DEUTERIUM AND HELIUM-3 OF SECONDARY ORIGIN AND THE RESIDUAL MODULATION OF COSMIC RAYS

REUVEN RAMATY*
NASA, Goddard Space Flight Center, Greenbelt, Maryland
AND
RICHARD E. LINGENFELTER†
Institute of Geophysics and Planetary Physics, University of California, Los Angeles
*Received April 19, 1968; revised July 22, 1968*

## ABSTRACT

Assuming that cosmic-ray deuterons and helium-3 nuclei are of secondary origin, we show that a unique determination of both the cosmic-ray path length and the residual interplanetary field modulation at solar minimum may be made from a comparison of the calculated and measured intensities of these two nuclei. This determination does not depend on any assumptions regarding either the source spectra or the unmodulated proton-to-alpha particle ratio of the primary cosmic rays. The production of deuterium and helium-3 by cosmic-ray interactions in the Galaxy is calculated by considering energy-dependent cross-sections, interaction kinematics, and demodulated cosmic-ray spectra. The resulting flux at the Earth is obtained by taking into account leakage from the Galaxy, ionization losses, nuclear breakup, and modulation. From a comparison of these calculations with the measured deuterium and helium-3 intensities at the Earth, we conclude that within the experimental uncertainties all the data can be understood in terms of an energy-independent, cosmic-ray path length of $4 \pm 1$ g cm$^{-2}$ and a residual interplanetary field modulation at solar minimum which above 600 MV is of the form $\exp(-\eta/R\beta)$ with $\eta = 0.35 \pm 0.15$ BV, where $R$ and $\beta$ are rigidity and velocity, respectively.

## I. INTRODUCTION

The abundance of deuterium and helium-3 in the cosmic rays was found to be significantly larger than that expected from the study of the universal abundance of elements (Fan *et al.* 1966*a;* Fan, Gloeckler, and Simpson 1966*b;* O'Dell *et al.* 1966; Biswas *et al.* 1967; Dennis *et al.* 1967; Freier and Waddington 1968). It has been suggested, therefore, that these isotopes are of secondary origin, produced by nuclear interactions of cosmic rays with the interstellar gas and that the comparison of the observed and calculated intensities of deuterium and helium-3 could determine the mean amount of material traversed by cosmic rays in interstellar space.

Previous studies of $d$ and $He^3$ production were made by Hayakawa, Ito, and Terashima (1958), Foster and Mulvey (1963), Badhwar and Daniel (1963), Dahanayake, Kaplon, and Lavakare (1964), Kuzhevskii (1966), Fan and co-workers (1966*a*, *b*), Fichtel and Reames (1966), Badhwar and Kaplon (1966), Biswas, Ramadurai, and Sreenivasan (1968), and Meyer, Hagge, and McDonald (1968). The mean cosmic-ray path lengths deduced from these studies range from a few g cm$^{-2}$ to more than 10 g cm$^{-2}$, and they may or may not be energy dependent. Even though these values are of the same order as the path length deduced from the observed abundances of Li, Be, and B (Shapiro and Silverberg 1968), the determination of the amount of material traversed by cosmic rays at low energies is seriously complicated by an unknown residual solar modulation.

The existence of such a residual modulation, active even at solar minimum, is indicated by the measurements of an interplanetary gradient, between the orbits of the Earth and Mars, in the proton and alpha-particle fluxes (O'Gallagher and Simpson

* NAS-NASA Postdoctoral Resident Research Associate.

† Research supported by the National Science Foundation under grant GP-849.

1967; O'Gallagher 1967). The measurement of this gradient, however, determines only the relative modulation over a distance of roughly an astronomical unit and not the total residual modulation, which, short of direct measurements over large distances in the solar system, remains essentially undetermined.

In a preliminary report of rather extensive calculations of deuterium and helium-3 production (Ramaty and Lingenfelter 1968), we suggested that because of the secondary origin of these nuclei and because of their different charge-to-mass ratio, a comparative study of $d$ and $He^3$ in the cosmic rays allows an essentially independent determination of both the amount of material traversed by cosmic rays and their total residual modulation in the interplanetary magnetic field. Unlike previous attempts to estimate the total modulation, this technique relies solely on the assumption that the observed $d$ and $He^3$ are of secondary origin and does not depend on any arbitrary assumption about the charge ratios or spectral shapes of the primary cosmic rays either in interstellar space or at their sources. In the present paper we give a detailed discussion of these calculations and conclusions.

The production spectra of deuterium and helium-3, resulting from the interaction of cosmic-ray protons, alpha particles, and medium nuclei with the interstellar gas, are calculated by taking into account the energy dependence of the cross-sections, the kinematics and the secondary energy distributions of the various interactions producing deuterons and helium-3 nuclei. Using these spectra, we evaluate the equilibrium $d$ and $He^3$ fluxes by considering leakage from the Galaxy, ionization losses, and nuclear breakup. The residual solar modulation is taken into account by first demodulating the observed primary cosmic-ray fluxes at the Earth, then by using these demodulated intensities to calculate the production of $d$ and $He^3$ in interstellar space, and finally by modulating the resultant secondary equilibrium fluxes with the same modulating function as used in the initial demodulation process. By comparing the resultant $d$ and $He^3$ spectra with the observations, it is demonstrated that the measured deuteron and helium-3 fluxes at the Earth can be best understood in terms of an energy-independent path length and a residual solar modulation which is both velocity and rigidity dependent.

## II. DEUTERON AND HELIUM-3 PRODUCTION

The rate of production of secondary nuclei by cosmic-ray interactions in the interstellar material may be written as

$$q_s(E_s) = 4\pi \sum_i \int dE j_i(E) n_i \sigma_i(E) F_i(E,E_s) , \qquad (1)$$

where $q_s$ is the production spectrum of secondary nuclei per second per gram of interstellar material; $E$ and $E_s$ are the energies per nucleon of the primary and secondary particles, respectively; $j$ is the equilibrium intensity in interstellar space of the interacting cosmic-ray nuclei; $n$ is the number of target nuclei per gram of interstellar material; $\sigma$ is the interaction cross-section; and $F(E,E_s)dE_s$ is the probability that a primary cosmic-ray nucleus of energy per nucleon $E$ will produce a secondary nucleus of energy per nucleon in $dE_s$ around $E_s$.

The production is summed over all interactions, $i$, which produce the secondary nucleus, $s$. The interactions which we have considered for the production of deuterium, helium-3, and tritium, which decays into helium-3, are listed in Table 1. Each of these interactions may also include the generation of pions.

The interstellar material is assumed to be composed of hydrogen, helium, and CNO nuclei in the ratio $1:10^{-1}:10^{-3}$ (Suess and Urey 1956; Cameron 1959).

We shall now provide detailed discussions of the primary cosmic-ray intensities, production cross-sections, and the kinematics and secondary energy spectra to be used in the evaluation of equation (1).

*a) Primary Cosmic-Ray Intensities*

The energy spectra of the various charge components of the primary cosmic radiation were measured near the Earth at solar minimum by Freier and Waddington (1965), Balasubrahmanyan *et al.* (1966*a*, *b*), Comstock, Fan, and Simpson (1966), Fan *et al.* (1966*b*), Hofmann and Winckler (1966), Ormes and Webber (1966), and Waddington and Freier (1966). The interstellar primary cosmic-ray intensities used to evaluate equation (1) are obtained by demodulating these measured spectra with a modulating function, $M$, of the form $\exp[-\eta/\beta f(R)]$, based on Parker's (1958) solar-wind model. The modulating parameter $\eta$, which is space and time dependent, defines the total residual solar modulation, $\beta$ is the particle velocity in units of $c$, and $f(R)$ is a function of magnetic rigidity and depends on the distribution of the interplanetary magnetic-field irregularities. It was first suggested by Dorman (1963) that $f(R)$ could be approximated by $f(R) = R_0$ for $R < R_0$ and $f(R) = R$ for $R > R_0$, where $R_0$ is a characteristic transition rigidity depending on the distribution of the magnetic irregularities. Subsequently, Jokipii (1966, 1968) and Jokipii and Coleman (1968) demonstrated that such a form is consistent with the measured power spectrum of the interplanetary field variations,

TABLE 1

DEUTERON AND HELIUM-3 PRODUCTION

| | Deuteron | | Helium-3 |
|---|---|---|---|
| 1 . | $p+H^1 \rightarrow d+\pi^+$ | 1.. | $p+He^4 \rightarrow He^3+d+(\pi)$ |
| 2 . | $p+He^4 \rightarrow d+He^3+(\pi)$ | 2.. | $\alpha+H^1 \rightarrow He^3+d+(\pi)$ |
| 3... | $\alpha+H^1 \rightarrow d+He^3+(\pi)$ | 3.. | $p+He^4 \rightarrow t+2p+(\pi)$ |
| 4.. | $p+He^4 \rightarrow d+2p+n+(\pi)$ | 4. | $\alpha+H^1 \rightarrow t+2p+(\pi)$ |
| 5... | $\alpha+H^1 \rightarrow d+2p+n+(\pi)$ | 5... | $\alpha+He^4 \rightarrow t+p+\alpha+(\pi)$ |
| 6... | $\alpha+He^4 \rightarrow d+p+n+\alpha+(\pi)$ | 6.. | $p+He^4 \rightarrow He^3+p+n+(\pi)$ |
| 7.. | $p+He^4 \rightarrow 2d+p+(\pi)$ | 7. | $\alpha+H^1 \rightarrow He^3+p+n+(\pi)$ |
| 8.. . | $\alpha+He^4 \rightarrow 2d+p+(\pi)$ | 8... | $\alpha+He^4 \rightarrow He^3+n+\alpha+(\pi)$ |
| 9.. | $\alpha+He^4 \rightarrow 2d+\alpha+(\pi)$ | 9.... | $p+CNO \rightarrow He^3+\ldots+(\pi)$ |
| 10.... . | $p+CNO \rightarrow d+\ldots+(\pi)$ | 10.... | $CNO+H^1 \rightarrow He^3+\ldots+(\pi)$ |
| 11..... | $CNO+H^1 \rightarrow d+\ldots+(\pi)$ | | |

with $R_0$ essentially time dependent and of the order of several hundred MV in 1965. With this functional form for $f(R)$, the modulating function mentioned above can be written as

$$\begin{aligned} M &= \exp(-\eta/R_0\beta), & R < R_0; \\ &= \exp(-\eta/R\beta), & R > R_0. \end{aligned} \tag{2}$$

Gloeckler and Jokipii (1966), Balasubrahmanyan, Boldt, and Palmeira (1967), O'Gallagher and Simpson (1967) and O'Gallagher (1967) have also shown that the measured temporal and spatial variations of cosmic rays in the interplanetary medium can be explained by such a modulation but have deduced different values for the modulating parameter $R_0$. Since there is no general agreement as to the value of $R_0$, and since the modulating parameters which define the total modulation may be different from the values obtained from the temporal and spatial variations mentioned above, we have treated both $\eta$ and $R_0$ as free parameters to be determined from the present study.

*b) Production Cross-Sections*

The deuteron-production cross-section for proton-proton interactions has been measured in considerable detail from threshold to a few BeV by Schulz (1952), Crawford

(1953), Stevenson (1953), Durbin, Loar, and Steinberger (1951), Fields *et al.* (1954), Stadler (1954), Baldoni *et al.* (1962), Guzhavin *et al.* (1964), Neganov and Parfenov (1958), Chapman *et al.* (1964), Fickinger *et al.* (1962), Pickup, Robinson, and Salant (1962), Smith *et al.* (1961), and Hart *et al.* (1962), and the theory of the interaction has been studied by Rosenfeld (1954). These cross-section data together with a smoothed curve used in the present calculation are shown in Figure 1.

The cross-sections for the production of deuterons, tritons, and helium-3 nuclei from the breakup of $He^4$ were measured in proton interactions with alpha particles at 28 MeV by Wickersham (1957), at 31 MeV by Bunch, Forster, and Kim (1964), at 32 MeV by Benveniste and Cork (1953), at 53 MeV by Cairns *et al.* (1964), at 55 MeV by Hayakawa *et al.* (1964), and at 95 MeV by Selove and Teem (1958), and in neutron interactions with alpha particles at 90 MeV by Tannenwald (1953), and at 300 MeV by

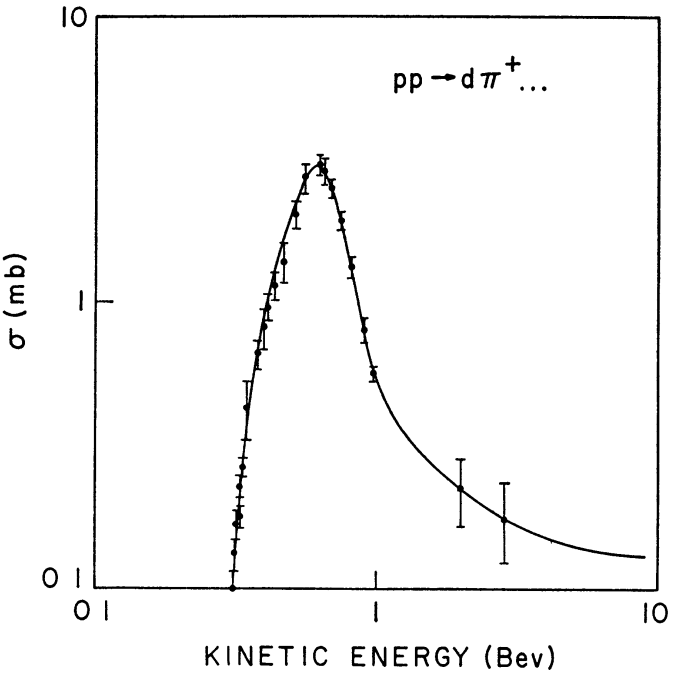


FIG. 1.—Deuteron-production cross-section for the reaction $H^1(p,d)\pi^+$

Moulthrop (1955) and Innes (1957). These data are shown in Figure 2. We have assumed that the $He^4$ breakup cross-sections at these energies are the same for incident protons as for neutrons. The measurement of the pickup cross-section by Tannenwald (1953) of $12 \pm 2.5$ mb for 90 MeV neutrons in the reaction $n\alpha \rightarrow dt$ and by Selove and Teem (1958) of $15 \pm 3$ mb for 95 MeV in the reaction $p\alpha \rightarrow d\mathrm{He}^3$ suggest that the Coulomb barrier for protons is not important at these energies and that these cross-sections are equal. At lower energies, particularly near the threshold, the Coulomb barrier is important, and the proton-pickup cross-section is much lower than that for neutrons, which shows a resonance at about 22.15 MeV.

Measurements of alpha-particle breakup were also made at 630 MeV by Kozadaev *et al.* (1960) and at 970 MeV by Riddiford and Williams (1960). These measurements differentiate between reactions having two, three, or more charge particles in the final state but do not completely distinguish between the various modes. Therefore, some assumptions must be made in order to obtain the deuteron, triton, and helium-3 yields. It was shown by Moulthrop (1955) and Innes (1957) that in 3-prong reactions (three charged particles in the final state) the ratios between the alpha-particle breakup modes

into singly charged fragments, $pt:pnd:dd:2p2n \approx 0.58:0.26:0.12:0.04$, are the same in both pion- and non-pion-producing reactions and that these rates are roughly independent of energy.

Using this relationship, and the fact that Kozadaev *et al.* (1960) did measure the non-pionic *pt* breakup, we can separate their 3-prong cross-section into partial cross-sections for these breakup modes for both pion- and non-pion-producing reactions. A similar treatment is applied to the data of Riddiford and Williams (1960) with the additional assumption that $\pi^0$ and $\pi^+$ production are roughly equal.

In order to reduce the 2-prong inelastic reactions which include the $d\mathrm{He}^3$ and $pn\mathrm{He}^3$ final states, we make three assumptions: (*a*) pion production without alpha-particle breakup constitutes roughly 10 per cent of the total pion-production cross-section at

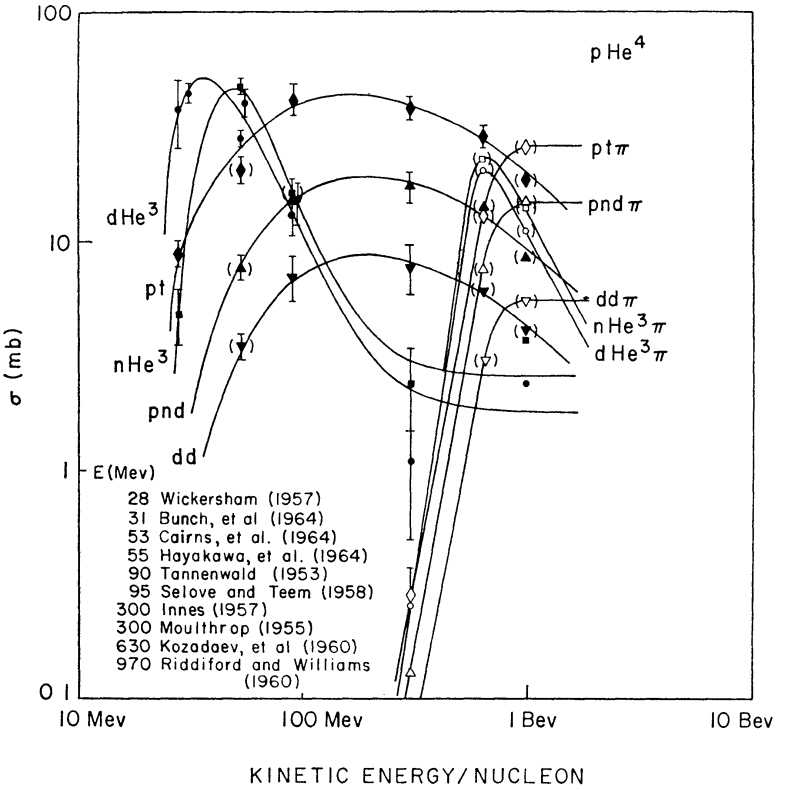


FIG. 2.—Deuteron-, triton-, and helium-3-production cross-sections for $p\mathrm{He}^4$ reactions

energies greater than 300 MeV, based on the measurements of Innes (1957); (*b*) $\pi^+$ and $\pi^0$ production are roughly equal; and (*c*) the $d\mathrm{He}^3$ and $pn\mathrm{He}^3$ final states are equally probable in pion-producing reactions, based on a similar equality found for non-pionic modes in the lower-energy measurements. The cross-sections thus deduced are shown in parentheses in Figure 2, together with the inferred energy-dependent partial cross-section for $p\alpha$ interactions.

In the absence of data on helium-4 breakup in $\alpha\alpha$ interactions, we have assumed that the same breakup modes occur and that their cross-sections are simply four times those in $\alpha p$ interactions at the same available kinetic energy in the center of mass frame. Since our calculations suggest that $\alpha\alpha$ interactions make a non-negligible contribution to *d* and $\mathrm{He}^3$ production, a measurement of the breakup cross-sections in the energy range around 100 MeV would be particularly valuable.

The deuteron-production cross-section in proton interactions with CNO nuclei was

measured at 18.5 MeV by Nadi and Riad (1964), at 20 MeV by Legg (1963), at 40 MeV by Kavaloski, Bassani, and Hintz (1963) and at 190 MeV by Bailey (1956). At higher energies the cross-section can be estimated from the $d/t$ yields calculated by Fraenkel (personal communication) and measured by Schwarzschild and Zupancic (1963). The tritium-production cross-section for these interactions was measured at 43 MeV by Cherny and Pehl (personal communication), at 150 MeV by Brun, Leforth, and Tarrago (1962), at 190 MeV by Bailey (1956), at 224, 300, 400, and 750 MeV by Honda and Lal (1960), at 450 MeV and 2.05 BeV by Currie, Libby, and Wolfgang (1956), at 2.2 BeV by Fireman and Rowland (1955), and at 6.2 BeV by Currie (1959). The helium-3-production cross-section in proton-CNO interactions is not well measured, but the measurements of Bailey (1956) at 190 MeV and the Monte Carlo calculations of Fraenkel

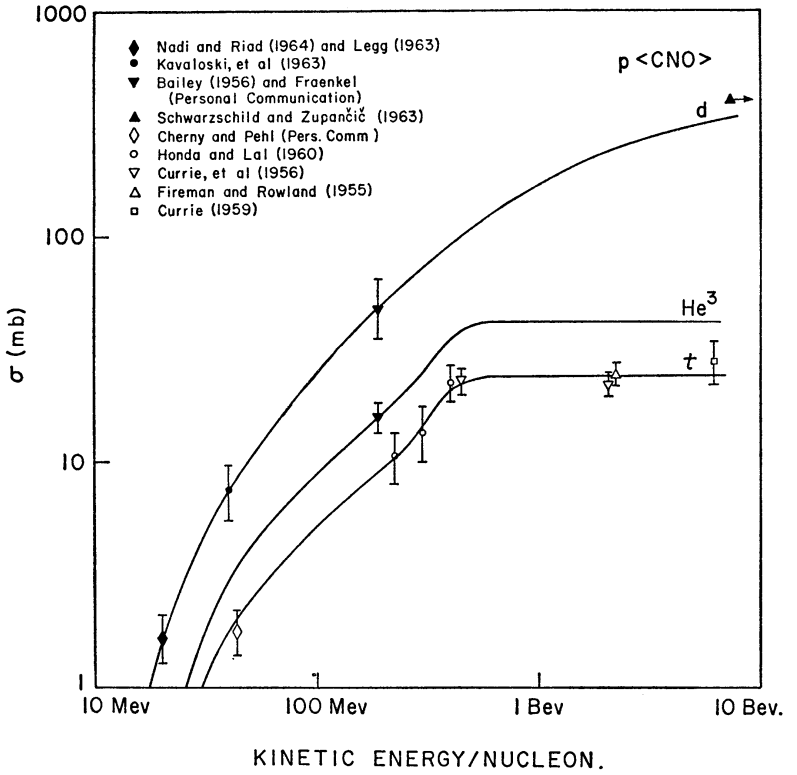


FIG. 3.—Deuteron-, triton-, and helium-3-production cross-sections for $p$CNO reactions

(personal communication) indicate that the $He^3/H^3$ yields are of the order of 1.7 from protons of energies between a hundred and several hundred MeV, and we have assumed that this ratio holds for all energies. These cross-sections, averaged to a mean value for CNO in the cosmic-ray nuclear ratio of 0.45:0.10:0.45 (Comstock *et al.* 1966) are shown in Figure 3.

### *c) Kinematics and Secondary Energy Spectra*

The distribution functions $F(E,E_s)$ can be determined from measurements of the angular and energy distributions of deuterons and helium-3 nuclei produced in nuclear interactions. Consider the interaction of an incident particle of mass $m_i$ and Lorentz factor, $\gamma = 1 + E/m_i$, with a stationary target nucleus of mass $m_t$. Such a reaction may produce two or more secondary particles. Consider one of these particles and let $p(\gamma,\gamma_s^*, \cos\theta^*)d\gamma_s^* d\cos\theta^*$ be the probability that in the center-of-mass frame it is emitted into $d\cos\theta^*$ around $\cos\theta^*$ with Lorentz factor in $d\gamma_s^*$ around $\gamma_s^*$. In terms of

this probability, the distribution function $F(\gamma,\gamma_s)$ may be written as

$$F(\gamma,\gamma_s) = \int d\gamma_s^* P(\gamma,\gamma_s^*, \cos\theta^*) \frac{d\cos\theta^*}{d\gamma_s} . \tag{3}$$

The laboratory Lorentz factor $\gamma_i$ is determined from the center-of-mass Lorentz factor and emission angle by

$$\gamma_s = \gamma_c\gamma_s^* + \{(\gamma_c^2 - 1)[(\gamma_s^*)^2 - 1]\}^{1/2} \cos\theta^* , \tag{4}$$

where $\gamma_c$ is the Lorentz factor of the center of mass

$$\gamma_c = \frac{\gamma m_i + m_t}{E'} = \frac{E'^2 + m_t^2 - m_i^2}{2m_tE'} , \tag{5}$$

and $E'$ is the total available energy in the center-of-mass frame

$$E' = (m_i^2 + m_t^2 + 2\gamma m_i m_t)^{1/2} . \tag{6}$$

Substituting $d\cos\theta^*/d\gamma_s$ from equation (4) into equation (3), we get

$$F(\gamma,\gamma_s) = (\gamma_c^2 - 1)^{-1/2} \int d\gamma_s^* [(\gamma_s^*)^2 - 1]^{-1/2} P(\gamma,\gamma_s^*, \cos\theta^*) . \tag{7}$$

If the final state consists of more than two particles, the Lorentz factor, $\gamma_s^*$, of one of the secondary particles having mass $m_s$ may have any value up to a maximum which is determined by the conservation of momentum and energy and is given by

$$\gamma_m^* = \frac{E'^2 + m_s^2 - m_r^2}{2m_sE'} , \tag{8}$$

where $m_r$ is the sum of the masses of all the other secondary particles. However, if the final state consists of only two particles, then $\gamma_s^* = \gamma_m^*$, and the probability distribution $P(\gamma,\gamma_s^*, \cos\theta^*)$ reduces to a delta function in $\gamma_s^*$, and equation (7) becomes

$$F(\gamma,\gamma_s) = \{(\gamma_c^2 - 1)[(\gamma_m^*)^2 - 1]\}^{-1/2} P(\gamma, \cos\theta^*) . \tag{9}$$

For the purpose of evaluating the integrals over $\gamma$ and $\gamma_s^*$ given in equations (1) and (3), we have to consider the ranges of the incident Lorentz factor $\gamma$ and the secondary Lorentz factor $\gamma_s^*$ which can contribute to a given laboratory Lorentz factor $\gamma_s$. Since $\gamma_c$ is uniquely determined by $\gamma$ and vice versa, the permissible range of $\gamma_c$ also determines that of $\gamma$. These ranges are determined by the requirements that $|\cos\theta^*| \leq 1$, and that $\gamma_s^* \leq \gamma_m^*$ for more than two particles, or $\gamma_s^* = \gamma_m^*$ for only two particles in the final state, respectively.

Using equation (4), we find that the restrictions on $\cos\theta^*$ imply

$$-1 < (\gamma_s - \gamma_c\gamma_s^*)\{(\gamma_c^2 - 1)[(\gamma_s^*)^2 - 1]\}^{-1/2} < 1 . \tag{10}$$

For a fixed $\gamma_s$, this inequality restricts $\gamma_c$ and $\gamma_s^*$ to the inside of a hyperbola given by

$$\gamma_c^2 + (\gamma_s^*)^2 + \gamma_s^2 - 2\gamma_c\gamma_s^*\gamma_s - 1 = 0 . \tag{11}$$

For illustration, such hyperbolas are shown by solid lines in Figure 4 for $\gamma_s = 1.01$, 1.1, and 2.0, corresponding to deuterons of roughly 10, 100, and 1000 MeV nucleon$^{-1}$, respectively. The three branches of each hyperbola are separated by the points ($\gamma_c = \gamma_s;\gamma_s^* = 1$) and ($\gamma_c = 1;\gamma_s^* = \gamma_s$). The value of $\cos\theta^*$ is $-1$ on the two branches which extend out to large values of $\gamma_c$ and $\gamma_s^*$ and $+1$ on the remaining branch. Inside of each hyperbola $\cos\theta^*$ has values between $+1$ and $-1$.

The dashed curves in Figure 4 are plots of $\gamma_m^*$ as a function of $\gamma_c$, determined from equations (5) and (8) for the reactions $H^1(p,d)\pi^+$, $He^4(p,d)He^3$, and $p(He^4,d)He^3$. At threshold $\gamma_m^* = 1$ and $\gamma_c = \gamma_{ct}$, which is the Lorentz factor of the center of mass at threshold. Since at threshold $E' = m_s + m_r$, from equation (5) we obtain

$$\gamma_{ct} = \frac{(m_s + m_r)^2 + m_t^2 - m_i^2}{2m_t(m_s + m_r)} . \tag{12}$$

As the incident energy increases above threshold, $\gamma_c$ and $\gamma_m^*$ also increase above their threshold values and $\gamma_m^*$ may or may not become greater than $\gamma_c$. The condition for this may be seen from the asymptotic behavior of $\gamma_m^*$ at large incident energies, $\gamma_m^* \sim (m_t/m_s)\gamma_c$. Thus if $m_t > m_s$, for $\gamma_c > \gamma_{cz}$, $\gamma_m^* > \gamma_c$, where $\gamma_{cz}$ is the value of $\gamma_c$ at which $\gamma_m^* = \gamma_c$. The value of $\gamma_{cz}$ can be directly evaluated from equations (5) and (8) and is given by

$$\gamma_{cz} = \frac{(m_s^2 - m_r^2) - (m_t^2 - m_i^2)}{2\{(m_s - m_t)[m_t(m_s^2 - m_r^2) - m_s(m_t^2 - m_i^2)]\}^{1/2}} . \tag{13}$$

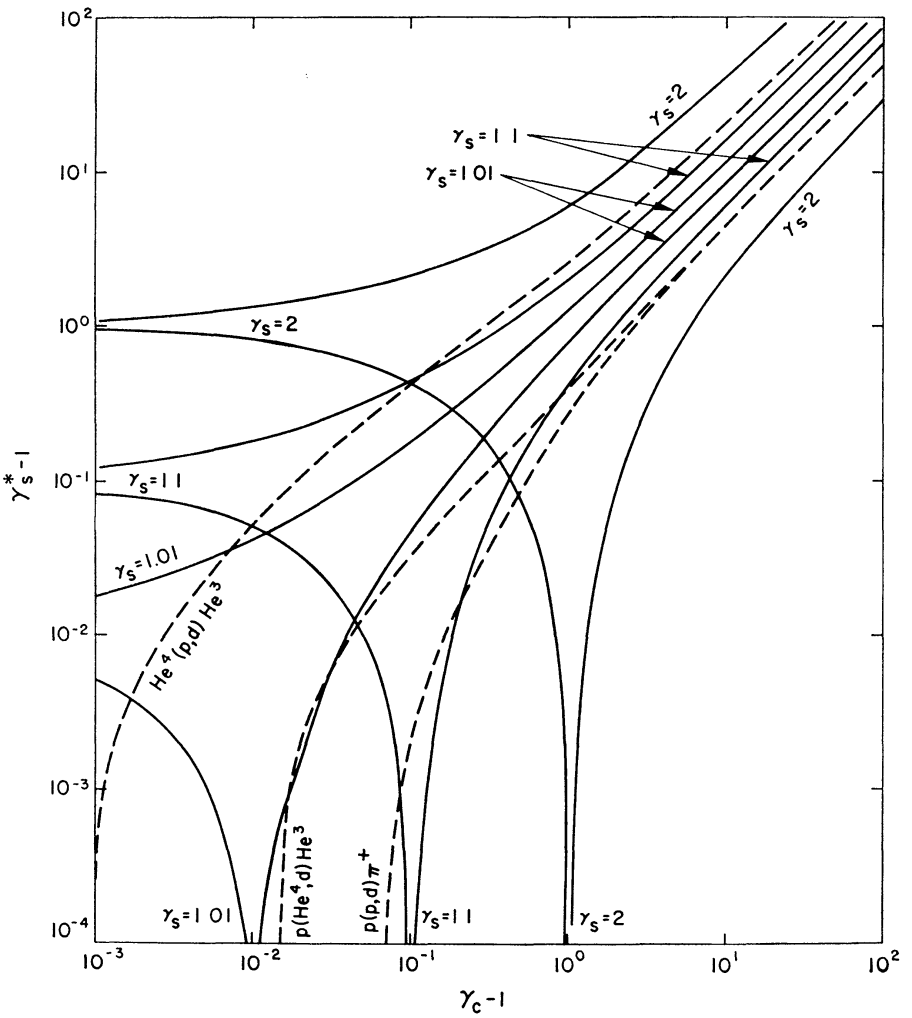


FIG. 4.—Ranges of the Lorentz factors of the center of mass, and of the secondary particle in the center of mass, $\gamma_c$ and $\gamma_s^*$, respectively, which for the indicated reactions can contribute to given secondary laboratory Lorentz factors, $\gamma_s$. The solid lines define the ranges of $\gamma_c$ and $\gamma_s^*$ which satisfy the inequalities (10), and the dashed lines represent $\gamma_m^*$ as a function of $\gamma_c$.

For values of $\gamma_c$ greater than $\gamma_{cz}$, secondary particles may be emitted in the laboratory frame into both the forward and backward cones. When $\gamma_s^*$ equals $\gamma_c$, particles emitted with $\theta^* = -\pi$ in the center-of-mass frame, have zero kinetic energy in the laboratory frame. However, if $m_t < m_s$, $\gamma_m^*$ can never equal $\gamma_c$ and in the laboratory frame, the secondary particle will always be emitted into the forward cone with non-vanishing energy.

The lower limit, $\gamma_{cl}$, of the range of values of $\gamma_c$ which may contribute to a given $\gamma_s$ is determined by the first intersection of $\gamma_m^*$ with the hyperbola corresponding to the given $\gamma_s$, as can be seen in Figure 4. Depending on whether $\gamma_c > \gamma_{ct}$ or $\gamma_s < \gamma_{ct}$, this corresponds to particles being emitted in the center-of-mass frame into the forward or backward directions.

The upper limit on $\gamma_c$, however, is not necessarily finite. The asymptotic forms of the two branches of the hyperbola corresponding to a given $\gamma_s$ are $\gamma_c[\gamma_s \pm (\gamma_s^2 - 1)^{1/2}]$ and, as mentioned above, for large $\gamma_c$, $\gamma_m^* \sim (m_t/m_s)\gamma_c$. Therefore, if

$$\gamma_s - (\gamma_s^2 - 1)^{1/2} < \frac{m_t}{m_s} < \gamma_s + (\gamma_s^2 - 1)^{1/2}\,, \tag{14}$$

$\gamma_m^*$ will remain always inside the hyperbola corresponding to $\gamma_s$. This inequality is equivalent to $\gamma_s > \gamma_s(\infty)$, where $\gamma_s(\infty)$ is equal to $\frac{1}{2}(m_t/m_s + m_s/m_t)$ and at large incident energies $\gamma_s(\infty)$ is the asymptotic value of the Lorentz factor of secondary particles, $\gamma_s$, emitted in the backward direction in the center-of-mass frame. Because of the relativistic addition of velocities, $\gamma_s(\infty)$ is independent of the incident energy, and therefore projectiles of the greatest energies may always produce secondary particles with $\gamma_s > \gamma_s(\infty)$, provided they are emitted close enough to the backward direction in the center-of-mass frame. In these cases, the upper limit, $\gamma_{cu}$, becomes infinite.

When $\gamma_c < \gamma_s(\infty)$ we have to consider separately the cases in which $m_t > m_s$ or $m_t < m_s$. For $m_t > m_t$ and two particles in the final state, the upper limit $\gamma_{cu}$ is determined by the second intersection of $\gamma_m^*$ and the hyperbola corresponding to $\gamma_s$. If there are more than two particles in the final state, however, $\gamma_{cu}$ becomes infinite. On the other hand, for $m_t < m_s$, $\gamma_{cu}$ is determined by the second intersection of $\gamma_m^*$ with the hyperbola corresponding to $\gamma_s$, regardless of the number of particles in the final state.

Finally, a further distinction exists between reactions having $m_t$ greater or smaller than $m_s$, namely that for $m_t > m_s$, the curve $\gamma_m^*$ will intersect every hyperbola at least once, whereas for $m_t < m_s$, $\gamma_s$ has to be greater than a minimal value, $\gamma_s(\min)$, in order that the corresponding hyperbola be intersected by $\gamma_m^*$. This can be seen by composing the curves of $\gamma_m^*$ for the reactions $He^4(p,d)He^3$ and $p(He^4,d)He^3$ in Figure 4. This minimal, laboratory Lorentz factor is obtained when $\gamma_s^* = \gamma_m^*$, and the secondary particle is emitted into the backward direction in the center-of-mass frame, $\theta^* = -\pi$. From equation (4) with $\gamma_s^* = \gamma_m^*$ and $\theta^* = -\pi$, we find that the derivative of $\gamma_s$ vanishes when

$$\left\{\gamma_c(\gamma_c^2 - 1)^{-1/2} - \gamma_m^*[(\gamma_m^*)^2 - 1]^{-1/2}\right\}\left\{\frac{d\gamma_m^*}{d\gamma_c} - \left[\frac{(\gamma_m^*)^2 - 1}{\gamma_c^2 - 1}\right]^{1/2}\right\} = 0\,. \tag{15}$$

The first term will never vanish since $\gamma_m^* < \gamma_c$; the laboratory Lorentz factor $\gamma_s$ will go through a minimum when the second term vanishes. The values of $\gamma_c$ and $\gamma_m^*$ which satisfy equation (15), $\gamma_c(\min)$ and $\gamma_m^*(\min)$, are obtained from equations (5) and (8) and are given by

$$\gamma_c\ (\min) = \frac{m_i(m_s^2 + m_t^2 - m_i^2 - m_r^2) - 2m_r(m_t^2 - m_i^2)}{2m_t[m_i(m_s^2 - m_r^2) - m_r(m_t^2 - m_i^2)]^{1/2}} \tag{16}$$

and

$$\gamma_m^*\ (\min) = \frac{m_r(m_t^2 + m_r^2 - m_s^2 - m_i^2) + 2m_i(m_s^2 - m_r^2)}{2m_s[m_i(m_s^2 - m_r^2) - m_r(m_t^2 - m_i^2)]^{1/2}}\,. \tag{17}$$

The incident kinetic energies per nucleon $E_{th}$, $E_z$, $E_{min}$ corresponding to $\gamma_{ct}$, $\gamma_{cz}$, and $\gamma_c(\text{min})$, as well as the secondary laboratory kinetic energies per nucleon $E_s(\text{th})$, $E_t(\text{min})$ and $E_s(\infty)$, corresponding to $\gamma_{ct}$, $\gamma_s(\text{min})$, and $\gamma_s(\infty)$, are shown in Table 2. (Note that at threshold $\gamma_s = \gamma_c = \gamma_{ct}$.)

For illustration, the range of possible secondary energies as a function of incident energy is shown in Figure 5 for a variety of deuteron-producing reactions. The curves represent the kinematic limits determined from equation (4) for $\cos\theta^* = \pm 1$ and form the envelope of permissible secondary energies corresponding to intermediate values of $\cos\theta^*$. The significance of the various minima and asymptotic limits listed in Table 2 may also be seen in Figure 5.

TABLE 2

KINETIC ENERGY (MeV nucleon$^{-1}$)

| | $E_{th}$ | $E_z$ | $E_{min}$ | $E_s$(th) | $E_s$(min) | $E_s(\infty)$ |
|---|---|---|---|---|---|---|
| *d*-producing reactions | | | | | | |
| $pp \rightarrow d\pi^+$ | 286.5 | | 312 4 | 69.1 | 63.9 | 234 1 |
| $p\alpha \rightarrow d$ He$^3$ | 23 0 | 27.7 | | 0 9 | | 230 2 |
| $\alpha p \rightarrow d$ He$^3$ | 23 0 | | 37 3 | 14 6 | 9.1 | 234 1 |
| $p\alpha \rightarrow d\ 2pn$ | 31 7 | 38.2 | | 1 3 | | 230 2 |
| $\alpha p \rightarrow d\ 2pn$ | 31 7 | | 51 6 | 20 1 | 12 5 | 234 1 |
| $p\alpha \rightarrow dd\ p$ | 29 9 | 36 1 | | 1 2 | | 230 2 |
| $\alpha p \rightarrow dd\ p$ | 29.9 | | 48 6 | 19 0 | 11.8 | 234.1 |
| $p$ O$^{16} \rightarrow d$ | 14 3 | 14.4 | | 0 1 | | 2847.9 |
| O$^{16}$ $p \rightarrow d$ | 14 3 | | 27.1 | 12 6 | 6 6 | 234.1 |
| He$^3$-producing reactions | | | | | | |
| $p\alpha \rightarrow$ He$^3$ $d$ | 23 0 | 37.3 | | 0 9 | | 37 8 |
| $\alpha p \rightarrow$ He$^3$ $d$ | 23.0 | | 27.7 | 14 6 | 12.2 | 622.8 |
| $p\alpha \rightarrow t\ 2p$ | 24.8 | 40.2 | | 1.0 | | 37.8 |
| $\alpha p \rightarrow t\ 2p$ | 24.8 | | 29.9 | 15 8 | 13.1 | 622 8 |
| $p\alpha \rightarrow$ He$^3$ $pn$ | 24.8 | 40 2 | | 1 0 | | 37.8 |
| $\alpha p \rightarrow$ He$^3$ $pn$ | 24.8 | | 29 9 | 15 8 | 13 1 | 622 8 |
| $p$ O$^{16} \rightarrow t$ | 16.2 | 16 4 | | 0 1 | | 1639 0 |
| $p$ O$^{16} \rightarrow$ He$^3$ | 16.2 | 16.4 | | 0 1 | | 1639 0 |
| O$^{16}$ $p \rightarrow t$ | 16 2 | | 23 0 | 14 3 | 10 1 | 622 8 |
| O$^{16}$ $p \rightarrow$ He$^3$ | 16 2 | | 23 0 | 14.3 | 10 1 | 622.8 |

The center-of-mass angular distribution of deuterons from the reaction $H(p,d)\pi^+$ was well measured and has been studied by Rosenfeld (1954) who showed that the $(\frac{3}{2},\frac{3}{2})$ interaction was dominant and that the distribution was therefore given by $\frac{1}{3} + \cos^2\theta^*$. Since this reaction also results in two bodies in the final state, the deuteron distribution function is then given directly from the angular distribution and equation (9):

$$F(\gamma,\gamma_s) = (\tfrac{1}{3} + \cos^2\theta^*)\{(\gamma_c^2 - 1)[(\gamma_m^*)^2 - 1]\}^{-1/2} . \tag{18}$$

The center-of-mass angular distribution of deuterons from the reaction $He^4(p,d)He^3$ was measured at 31 MeV by Bunch *et al.* (1964), at 55 MeV by Hayakawa *et al.* (1964), and at 95 MeV by Selove and Teem (1958). These measurements are shown in Figure 6, and they can be fitted in detail by the model of Smith and Ivash (1962) based on the distorted-wave Born approximation with diffuse-well nuclear optical potentials. For the purposes of this calculation, however, we have fitted the distribution by functions of the form:

$$P(\gamma, \cos\theta^*) = \frac{\exp[-(1 - \epsilon\cos\theta^*)/\cos\theta_0]}{\cos\theta_0[1 - \exp(-2/\cos\theta_0)]} , \tag{19}$$

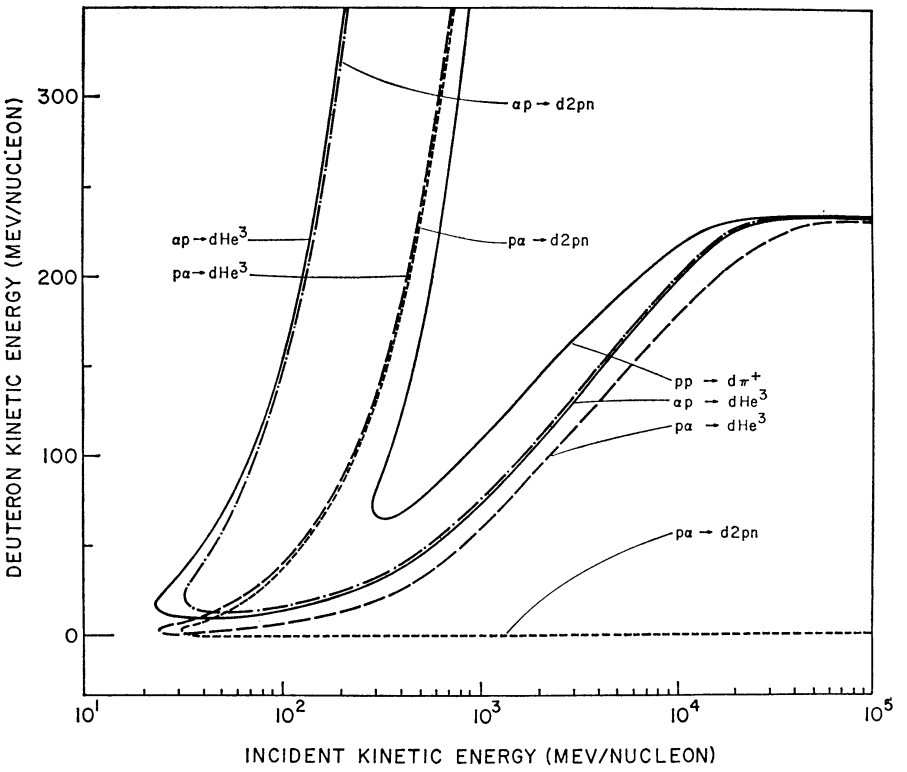


FIG. 5.—Ranges of the incident kinetic energies per nucleon which can contribute to a given secondary energy for the indicated deuteron-producing reactions. These ranges are determined from the requirements that $\cos\theta^* \leq 1$ and that the deuteron Lorentz factor in the center of mass be less than or equal to its maximum value determined from the conservation of energy and momentum.

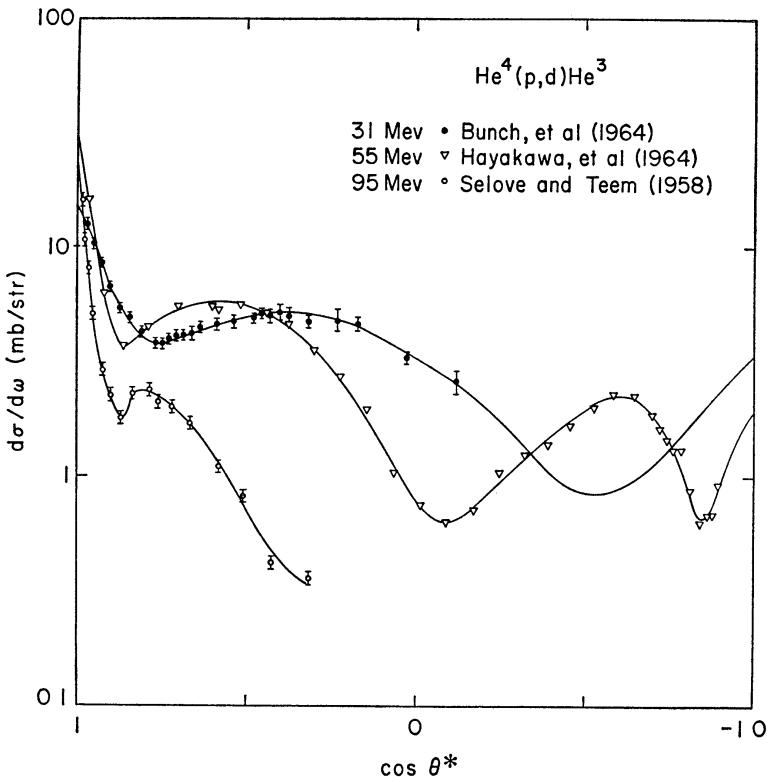


FIG. 6.—Angular distribution in the center of mass of deuterons from the reaction $He^4(p,d)He^3$ for various incident proton energies.

where $\cos\theta_0$ depends on the incident Lorentz factor $\gamma$. In the incident energy region of 30–90 MeV nucleon$^{-1}$, $\cos\theta_0$ can be well fitted by

$$\cos\theta_0 = \exp[9.38(\gamma - 1)] , \tag{20}$$

and we assumed this energy dependence for all values of $\gamma$ considered.

Since this reaction results in two bodies in the final state, the distribution function $F(\gamma,\gamma_s)$ for both deuterons and helium-3 nuclei is determined from equations (9) and (19). The parameter $\epsilon$ is $+1$ in the reactions $He^4(p,d)He^3$ and $H^1(a,He^3)d$ and is $-1$ in the reactions $H^1(a,d)He^3$ and $He^4(p,He^3)d$.

Above the pion-production threshold the more complex reactions leading to $dHe^3\pi^0$ and $dt\pi^+$ also become significant, as can be seen from the cross-sections shown in Figure 2. It has been shown by Riddiford and Williams (1960), however, that pions produced in proton-helium reactions are ejected as from the collision of free nucleons. Because of this, we have assumed that, kinematically, the $dHe^3\pi^0$ and $dt\pi^+$ reactions are similar to the reaction $H(p,d)\pi^+$, and therefore the distribution functions $F(\gamma,\gamma_s)$ are given by equation (18), where $\gamma_c$ and $\gamma_m{}^*$ are determined by equations (5) and (8) with $m_i = m_t = m_p$, $m_c = m_d$, and $m_r = m_\pi$.

The energy spectra in the laboratory frame of deuterons from *pnd* breakup of $He^4$ and of tritons from *pt* breakup of $He^4$ were measured by Tannenwald (1953) and by Innes (1957) for incident neutrons of 90 and 300 MeV, respectively. These data are shown in Figure 7, normalized to a unit integral. As can be seen, within the experimental uncertainties, the triton spectrum from the multibody *pt* breakup of $He^4$ is independent of the incident neutron energy and can be fitted by a simple exponential of the form: $\exp(-E_t/E_0)$, where $E_t$ is the triton kinetic energy per nucleon and $1/E_0$ is equal to 0.27 (MeV nucleon$^{-1}$)$^{-1}$. Similarly, the deuteron spectrum may be fitted by an exponential with $1/E_0 = 0.063$ (MeV nucleon$^{-1}$)$^{-1}$.

These spectra indicate that in the laboratory frame the multinucleon fragments tend to be produced predominantly with low energies. This will happen if the angular and Lorentz-factor distributions in the center of mass are peaked in the backward direction and around Lorentz factors which are about equal to the Lorentz factor of the center of mass. Assuming that the characteristic energy, $E_0$, is independent of the incident energy, the exponential distribution in kinetic energy per nucleon may be transformed into an exponential distribution in the center of mass angle, $\theta^*$. We assumed, therefore, that for the multibody reactions, $He^4(p,p')npd$, *dd*, *pt* and $n He^3$, the probability distribution function $P(\gamma,\gamma_s{}^*, \cos\theta^*)$ is given by

$$P(\gamma,\gamma_s{}^*, \cos\theta^*) = \frac{\exp[-(1 - \epsilon\cos\theta^*)/\cos\theta_0]}{\cos\theta_0[1 - \exp(-2/\cos\theta_0)]}\,\delta(\gamma_s{}^* - \langle\gamma_s{}^*\rangle) , \tag{21}$$

where in *pa* interactions, the parameter $\epsilon$ equals $-1$ and $\langle\gamma_s{}^*\rangle = \gamma_m{}^*$ for $\gamma_c < \gamma_{cz}$ and $\langle\gamma_s{}^*\rangle = \gamma_c$ for $\gamma_c > \gamma_{cz}$, and in *ap* interactions, $\epsilon = +1$, and the mean Lorentz factor $\langle\gamma_s{}^*\rangle$ is the same as in *pa* interactions for the same total available energy in the center of mass.

Using equations (4) and (9) with both $\gamma_s{}^*$ and $\gamma_m{}^*$ replaced by $\langle\gamma_s{}^*\rangle$, we find that the laboratory distribution function $F(\gamma,\gamma_s)$ becomes

$$F(\gamma,\gamma_s) = \exp\left[\frac{\epsilon(\gamma_s - \gamma_c\langle\gamma_s{}^*\rangle)}{\cos\theta_0[(\gamma_c{}^2 - 1)(\langle\gamma_s{}^*\rangle^2 - 1)]^{1/2}} - \frac{1}{\cos\theta_0}\right] \Big/ \times \{\cos\theta_0[1 - \exp(-2/\cos\theta_0)][(\gamma_c{}^2 - 1)(\langle\gamma_s{}^*\rangle^2 - 1)]^{1/2}\} . \tag{22}$$

In terms of the characteristic energy, $E_0$, defined above, $\cos\theta_0$ is given by

$$\cos\theta_0 = \frac{E_0}{m_p[(\gamma_c{}^2 - 1)(\langle\gamma_s{}^*\rangle^2 - 1)]^{1/2}} . \tag{23}$$

Since $E_0$ is independent of the incident energy, the energy dependence of cos $\theta_0$ is determined solely by $\gamma_c$ and $\gamma_s$.

We have also assumed the same distribution function, given by equation (22), for the multibody reactions *npd*, *dd*, *pt* and *n*He$^3$ when pions are produced.

There are no measurements of *d*, *t*, or He$^3$ production by $\alpha\alpha$ reactions. We have assumed arbitrarily that the breakup products of each He$^4$ nucleus effectively cluster together allowing us to treat the interaction as a two-body process with the two "clusters" having an isotropic angular distribution in the center-of-mass system. Thus, from

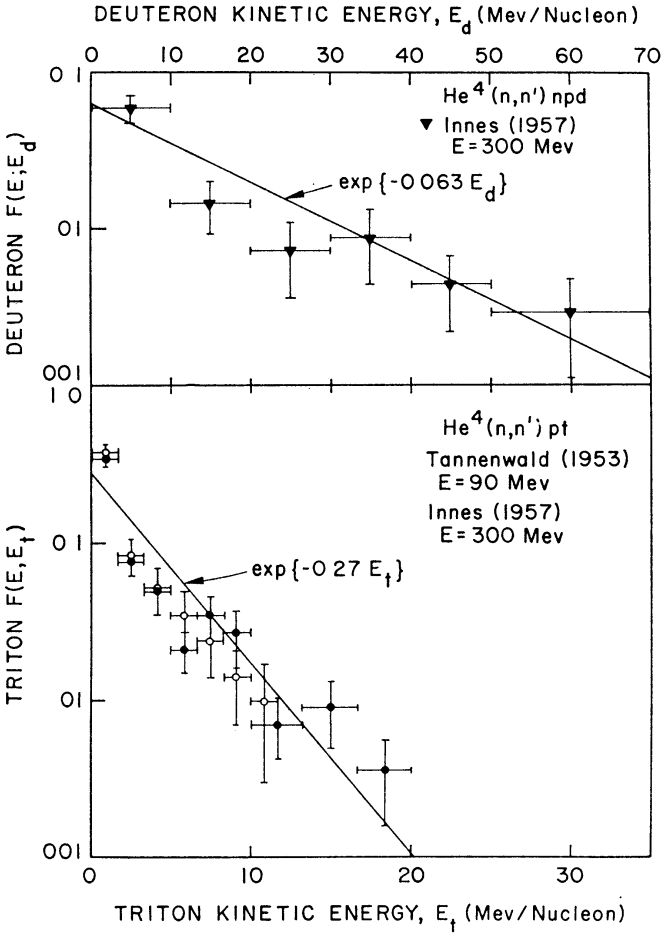


FIG. 7.—Energy distribution in the laboratory frame of deuterons and tritons from the multibody breakup of He$^4$.

equations (4)–(9), with $m_i = m_t = m_s = m_r$, we derive the distribution function for *d*, *t*, and He$^3$ produced in $\alpha\alpha$ reactions with and without pion production:

$$F(\gamma,\gamma_s) = (\gamma - 1)^{-1} . \tag{24}$$

The measurements of Bailey (1956) of the spectra of deuterons and helium-3 produced by 190 MeV protons on carbon are shown in Figure 8, normalized for unit integral. As can be seen, these spectra have the same form as those shown in Figure 7, and can also be fitted by an exponential characterized by $1/E_0 = 0.14$ (MeV nucleon$^{-1}$)$^{-1}$. Assuming that the triton distribution also has this form and that $E_0$ is independent of incident energy, the *d*, *t*, and He$^3$ distributions for $p$CNO reactions are the same as those given by equations (22) and (23).

*d) Production Spectra*

The rate of production per gram of interstellar material of deuterons and helium-3 nuclei as a function of secondary kinetic energy per nucleon can now be calculated by using the demodulated cosmic-ray spectra, production cross-sections, and the secondary energy distributions discussed above. We have performed these calculations for a variety of modulating parameters $\eta$ and $R_0$, and in general the absolute production increases with increasing $\eta$ but is quite insensitive to variations in $R_0$. The relative contribution of the various production reactions, however, is not strongly dependent on the assumed modulating parameters. For illustration, we show in Figures 9 and 10 the deuteron- and

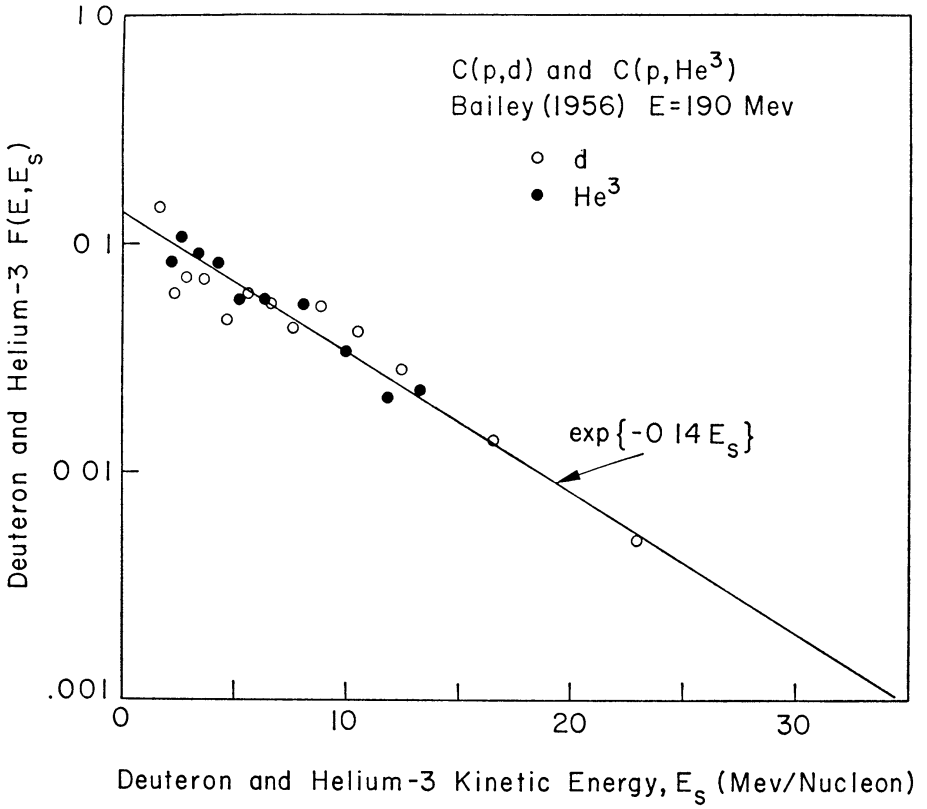


FIG. 8.—Energy distributions in the laboratory frame of deuterons and helium-3 nuclei from proton-carbon interactions.

helium-3-production spectra, respectively, for $\eta = 350$ MV and $R_0 = 0$. As can be seen from Figure 9, deuterons of energies less than about 70 MeV nucleon$^{-1}$ are produced with equal probability by cosmic-ray helium-4 on hydrogen in the pickup reaction $H(He^4, d)He^3$ and by cosmic-ray protons in the multibody breakup of helium; deuterons in the energy range from about 70 to 200 MeV nucleon$^{-1}$ are produced mainly in the $(\frac{3}{2},\frac{3}{2})$ resonance reaction of cosmic-ray protons on hydrogen, $H(p,d)\pi^+$; and deuterons of energy greater than about 200 MeV nucleon$^{-1}$ are produced with roughly equal probability by the multibody breakup reactions of cosmic-ray helium-4 on hydrogen. It should also be noted that the $\alpha\alpha$ reactions, under the assumptions made above, contribute approximately 20 per cent of the total deuteron production at all energies, and, because of the lack of experimental data on the cross-sections and kinematics of these reactions, an uncertainty of this order is introduced in the calculation from this source alone.

From Figure 10 we also see that helium-3 nuclei of energies less than about 40 MeV nucleon$^{-1}$ are produced principally by cosmic-ray helium-4 on hydrogen in the pickup reaction $H^1(He^4, He^3)d$, as are the low-energy deuterons, while helium-3 nuclei of higher energies are produced predominantly by the breakup of cosmic-ray helium-4 in the reaction $H^1(He^4, t)2p$, the tritium decaying to helium-3. The $\alpha\alpha$ reactions also produce about 20 per cent of the helium-3 and introduce a corresponding uncertainty in the total production.

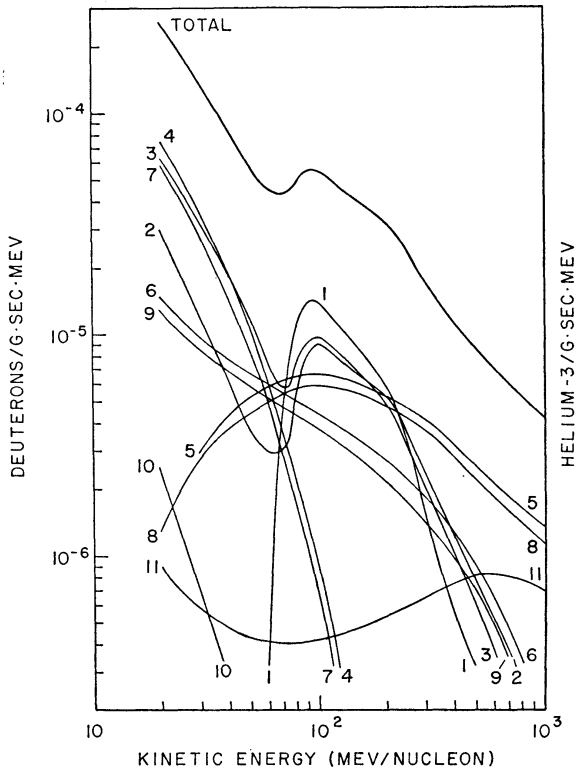


FIG 9

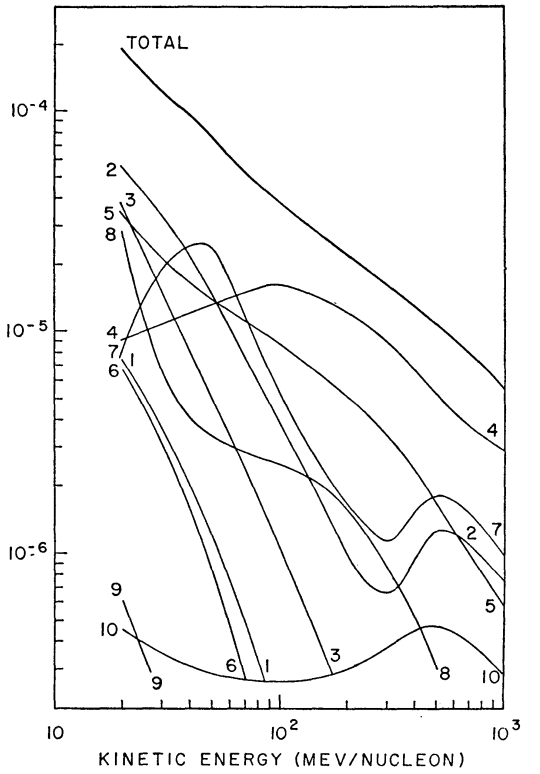


FIG 10

FIG. 9.—Deuteron-production spectra per gram of interstellar material for the various modes shown in Table 1. These spectra were computed for a demodulated cosmic-ray intensity with $\eta = 350$ MV and $R_0 = 0$.

FIG. 10.—Helium-3-production spectra per gram of interstellar material for the various modes shown in Table 1. These spectra were computed for a demodulated cosmic-ray intensity with $\eta = 350$ MV and $R_0 = 0$.

## III. DEUTERON AND HELIUM-3 FLUXES AT THE EARTH

From the rates of deuterium and helium-3 production in the interstellar medium, calculated above, we may now determine the equilibrium density of these secondaries in the Galaxy and then, taking into account modulation, the flux of the $d$ and $He^3$ nuclei at the Earth. The equilibrium densities of these nuclei in the Galaxy can be obtained by solving a steady-state continuity equation in energy space which takes into account leakage from the Galaxy, ionization losses, and nuclear breakup of the secondaries.

$$\frac{u_s}{\tau_L} + \frac{u_s v}{\lambda_d} + \frac{\partial}{\partial E}\left[\frac{dE}{dt} u_s\right] = \rho q_s(E) , \qquad (25$$

where $u_s$ is the secondary cosmic-ray equilibrium density; $q_s$ is the secondary production rate calculated above, per gram of interstellar material; $\rho$ is the density of interstellar

material in g cm$^{-3}$; $\tau_L$ is the leakage lifetime from the Galaxy; $dE/dt$ is the rate of energy loss due to ionization; and $\lambda_d/v$ is the mean lifetime against nuclear breakup. The solution of this equation can be written as

$$u_s(E) = \frac{\rho}{|dE/dt|} \int_E^\infty dE' q_s(E') \exp\left(-\int_E^{E'} \frac{dE''}{\tau |dE/dt|}\right), \tag{26}$$

where $\tau$ is the effective lifetime against leakage and nuclear breakup and is given by

$$\tau = \left(\frac{1}{\tau_L} + \frac{v}{\lambda_d}\right)^{-1}. \tag{27}$$

A more general expression for $u_s$, which under an appropriate simplification reduces to equation (26) given above, can be obtained by introducing a probability distribution per unit time, $P(t)$, such that $P(t)dt$ is the probability that an observed particle (at $t = 0$) was produced at a time $t$ in the past. In terms of this probability, the number of particles of energy in $dE$ around $E$ which were produced in the time interval $dt$ around $t$, with energies in $dE'$ around $E'$, is given by

$$du_s(E) = \rho q_s(E') \frac{dE'}{dE} P(t) dt, \tag{28}$$

where the energies $E$ and $E'$, the time interval $t$ and the energy loss rate $dE/dt$ have to satisfy the following relationship:

$$t = \int_E^{E'} \frac{dE''}{|dE/dt|}. \tag{29}$$

Equation (28) can be integrated by assuming that the rate of particle production $\rho q(E)$ is time independent. By changing the variable of integration from $t$ to $E'$, we find that the equilibrium density $u_s(E)$ is given by

$$u_s(E) = \frac{\rho}{|dE/dt|} \int_E^\infty dE' q_s(E') P\left(\int_E^{E'} \frac{dE''}{|dE/dt|}\right). \tag{30}$$

Equation (30) is similar to equation (26) given above, except that the exponential distribution is replaced by the more general expression, $P(t)$. The functional form of this expression, however, depends on a variety of factors, such as the spatial distribution of the sources, the nature of particle propagation from the sources to the Earth, and the properties of the trapping volume of the particles.

In the present study we have assumed a simple exponential distribution, $P(t) = e^{-t/\tau}$. Such a form is valid for the sudden losses resulting from nuclear breakup, and it might be a good approximation to a physical situation in which the sources are uniformly distributed in a trapping volume of radius $a$, from which cosmic rays escape by diffusion caused by scattering off magnetic irregularities. The leakage lifetime $\tau_L$, mentioned above, may then be written as $\tau_L = a^2/(2\lambda_L v)$ where $\lambda_L$ is the scattering, mean free path. For such an exponential distribution, equation (30) becomes equivalent to equation (26).

We now consider the numerical evaluation of equation (26). The energy loss rate $dE/dt$ due to ionization can be replaced by $\rho v dE/d\bar{R}$, where $R(E)$ are charged particle ranges given by Barkas and Berger (1964). The deuteron-breakup cross-section varies with energy but since we find that the lifetime $\tau$ is determined principally by leakage, we have taken it to be a constant of 170 mb which corresponds to the average value over the energy range 10–100 MeV nucleon$^{-1}$ (Van Oers 1963; Davison *et al.* 1963). The

helium-3-breakup cross-section is much smaller yet and hence was neglected. The breakup mean path length, $\lambda_d$, is given by $\lambda_d = (\sigma_d N_a \rho)^{-1}$, where $N_a$ is Avogadro's number.

Introducing a mean path length against leakage, $x = \rho v \tau_L$, we can rewrite equation (26) as

$$j_s(E) = \frac{dR/dE}{4\pi} \int_E^\infty dE' q_s(E') \exp\left[-\int_E^{E'} \left(\frac{1}{x} + \sigma_d N_a\right) \frac{dR}{dE} dE''\right], \qquad (31)$$

where $j_s(E)$ is the secondary cosmic-ray equilibrium intensity in interstellar space. We have evaluated equation (31) for a variety of production spectra, $q_s(E)$, corresponding to a range of values of the modulating parameters $\eta$ and $R_0$, defined above. We have

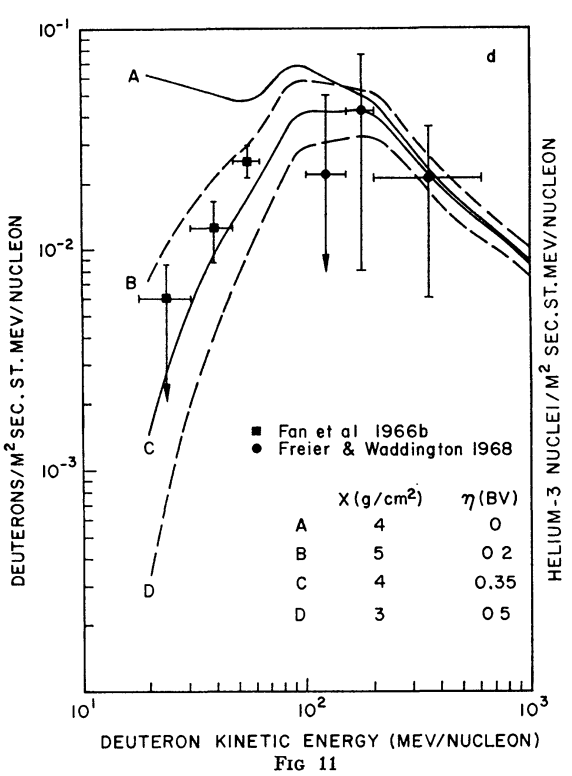


FIG 11

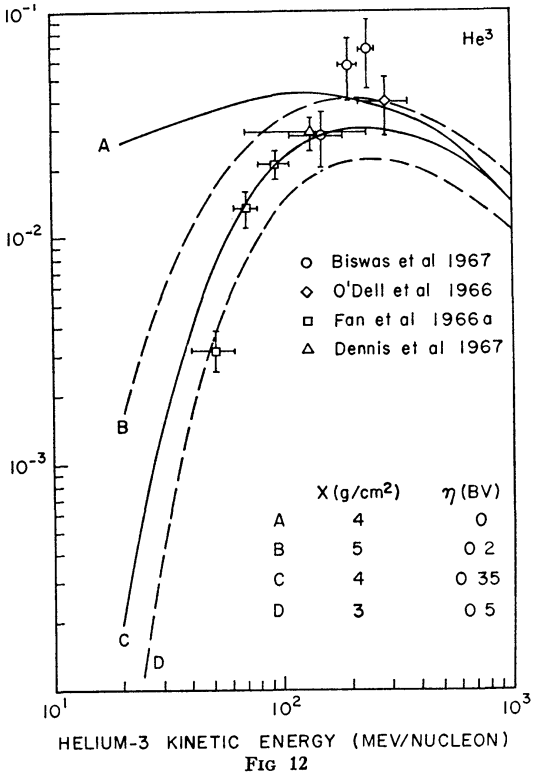


FIG 12

FIG. 11.—Observed intensity of deuterons, together with the calculated deuteron intensities at the Earth for various values of interstellar path lengths and modulating parameters.

FIG. 12.—Observed intensity of helium-3 nuclei, together with the calculated helium-3 intensities at the Earth for various values of interstellar path lengths and modulating parameters.

then obtained the $d$ and $He^3$ intensities at the Earth by modulating the resultant equilibrium spectra in interstellar space with the same modulating function as that used in the demodulation process. The results of these calculations, for $R_0 = 0$ and for several values of the mean path length $x$ and the modulating parameter $\eta$, are shown in Figures 11 and 12 for deuterons and helium-3 nuclei, respectively.

The net effect of the process of demodulation and the subsequent modulation, described above, is a decrease of the secondary intensity, because secondaries of a given energy are produced by primaries of higher energy which are therefore less modulated than the secondaries which they produce. This can be seen in Figures 11 and 12 from a comparison of curves $A$ and $C$, for zero modulation and modulation characterized by $\eta = 0.35$ BV. Also shown in Figures 11 and 12 are measurements at the Earth of deuterons and $He^3$ nuclei.

In comparing these data with our calculations, we first consider the case of zero residual modulation. As can be seen from curve $A$, we find that for a cosmic-ray path length of about 4 g cm$^{-2}$ and zero modulation, the calculated $d$ and He$^3$ intensities at energies greater than about 200 MeV nucleon$^{-1}$ are in good agreement with the measured intensities (O'Dell *et al.* 1966; Biswas *et al.* 1967; Dennis *et al.* 1967; Freier and Waddington 1968). A sensitive determination of the mean leakage path length, $x$, can be made only at these higher energies (>150 MeV nucleon$^{-1}$), where the range of $d$ and He$^3$ nuclei against ionization losses is greater than the values of $x$ investigated. At these energies the calculated equilibrium flux is determined principally by leakage from the Galaxy, and the intensity is directly proportional to $x$. At lower energies the ranges of $d$ and He$^3$ nuclei become much smaller than the 4 g cm$^{-2}$ leakage path length, and thus the calculated equilibrium is determined principally by ionization losses. As can be seen from curve $A$ at these lower energies, the calculated $d$ and He$^3$ intensities are much greater than the measured values (Fan *et al.* 1966*a*, *b*). For example, at 50 MeV nucleon$^{-1}$, where the range of an He$^3$ nucleus is 1 g cm$^{-2}$, this discrepancy amounts to more than an order of magnitude, and thus in order to account for the observed intensity at this energy, $x$ would have to be about 0.1 g cm$^{-2}$. This requires a very strong variation in the path length (of the order $x \propto E^3$) which seems rather unlikely. We therefore conclude that the measured spectra are probably not the result of an energy-dependent leakage path length. On the other hand, the comparison of curves $B$, $C$, and $D$ with the $d$ and He$^3$ data suggests that these spectra can be understood easily in terms of a residual interplanetary field modulation at solar minimum. This conclusion is supported by the observed gradient in the cosmic-ray intensity between the orbits of the Earth and Mars (O'Gallagher and Simpson 1967; O'Gallagher 1967).

The rigidity dependence of this residual modulation, however, is not well known, and as discussed above, there are significant disagreements among the various experimenters as to the energy dependence of the observed cosmic-ray spatial and temporal variations. According to Jokipii and Coleman (1968) the observed power spectrum of the interplanetary field variations indicates that the function $f(R)$, defined above, can be represented by a power law in $R$ with a varying spectral index, ranging from about $-0.5$ at low rigidities to $-2$ at high rigidities. Within the experimental errors, this would be consistent with the modulating function given by equation (2) with $R_0$ of the order of 600 MV. Such a rigidity-dependent modulation is indeed demanded by the observed deuteron and helium-3 data. As can be seen from curves $A$ in Figures 11 and 12, the calculated $d$/He$^3$ ratio at, for example, 50 MeV neucleon$^{-1}$ for zero residual modulation is about 1.3, whereas the measured ratio at the same energy per nucleon is perhaps as great as 6. Such a difference could result from a modulation of the form $\exp(-\eta/R\beta)$, as given by equation (2) for $R > R_0$. Since at the same energy per nucleon, deuterons have a higher rigidity and hence are less modulated than He$^3$ nuclei, such a rigidity-dependent modulation would increase the calculated $d$/He$^3$ ratio. Thus, the comparison of the $d$ and He$^3$ measurements with curve $A$ suggests not only the necessity of some residual modulation but also that above a rigidity of about 600 MV this modulation is velocity as well as rigidity dependent. Because of this, we wish to suggest that the comparison of future measurements of the $d$/He$^3$ ratio with the calculations described in the present paper could determine more accurately the charge dependence and energy spectrum of the residual solar modulation.

Since the present calculations do not depend on processes occurring below rigidities of about 600 MV, we have calculated the $d$ and He$^3$ spectra at the Earth for $R_0 = 0$, and a range of values of $x$ and $\eta$, thereby determining the values of these parameters which best fit the observed intensities. Within the experimental uncertainties, we find that the available data on both the deuterons and helium-3 nuclei can be best fitted by an energy-independent path length, $x = 4 \pm 1$ g cm$^{-2}$, and a residual modulation of the form $\exp(-\eta/R\beta)$ characterized by $\eta = 0.35 \pm 0.15$ BV. This can be seen by the best-fitting curve $C$ and the limiting curves $B$ and $D$ in Figures 11 and 12.

The $d$/He and $He^3$/He ratios derived from the present calculations are shown in Figures 13 and 14. Biswas *et al.* (1968) have recently concluded that the energy dependence of the $He^3$/He ratio can be accounted for only by an energy-dependent path length. However, as can be seen from these figures, our calculations show that both $He^3$/He and $d$/He ratios can be explained by an energy-independent, path-length distribution coupled with a residual solar modulation, which above about 600 MV is both velocity and rigidity dependent and is of the form exp $(-\eta/R\beta)$.

Finally we shall examine the implications of the interstellar cosmic-ray path length and residual interplanetary modulation on the primary cosmic-ray source spectra. Using the cosmic-ray propagation model assumed in the preceding calculations, we compute

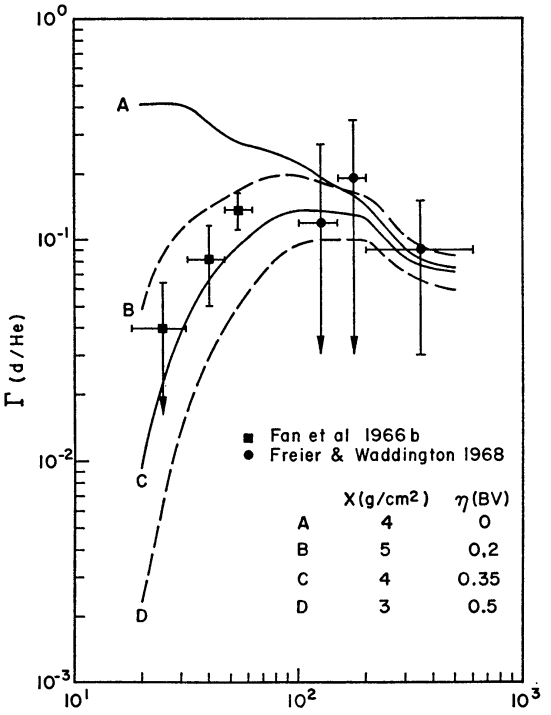


FIG 13

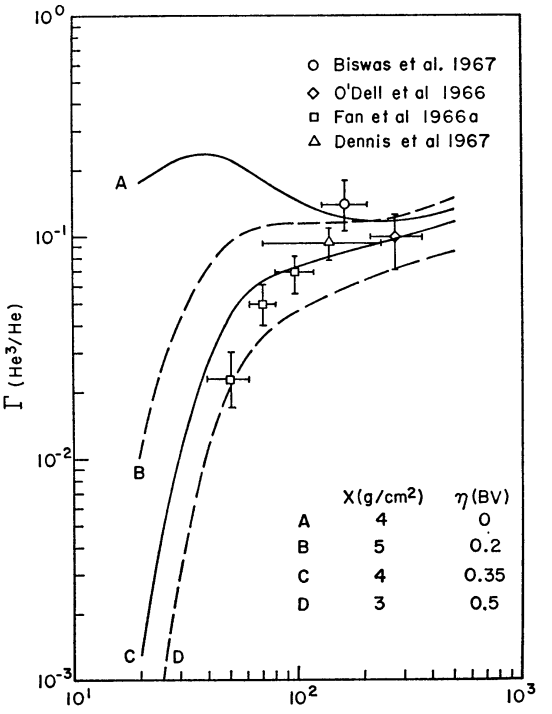


FIG. 14

FIG. 13.—Observed ratio of deuterons to helium nuclei, together with the calculated $d$/He ratios at the Earth for various values of interstellar path lengths and modulating parameters.

FIG. 14.—Observed ratio of helium-3 to helium nuclei, together with the calculated $He^3$/He ratios at the Earth for various values of interstellar path lengths and modulating parameters.

the interstellar equilibrium intensity of primary protons and alpha particles resulting from a homogeneously distributed galactic source with a given energy spectrum. Such spectra resulting from sources which are power laws in kinetic energy per nucleon, rigidity, and total energy per nucleon are shown in Figure 15 by curves *I*, *II*, and *III*, respectively, for $x = 4$ g cm$^{-2}$. For comparison we have demodulated the observed solar-minimum proton and alpha-particle spectra with the modulating function given above ($\eta = 0.35$ BV), and the resultant interstellar proton and alpha-particle spectra are also shown in Figure 15. These demodulated curves extend down to kinetic energies per nucleon corresponding to a rigidity of 600 MV, below which the results of the present calculations cannot be meaningfully applied. Above 200 MeV nucleon$^{-1}$ both the demodulated proton and alpha-particle spectra are consistent with a cosmic-ray source which is a power law in total energy (curve *III*) whereas below this energy the alpha-particle spectrum lies above this curve. If significant, this change of spectral shape may

reflect either a similar change in the spectra of the cosmic-ray sources or may be caused by a variety of effects such as solar or stellar acceleration and production by nuclear interactions in interstellar space.

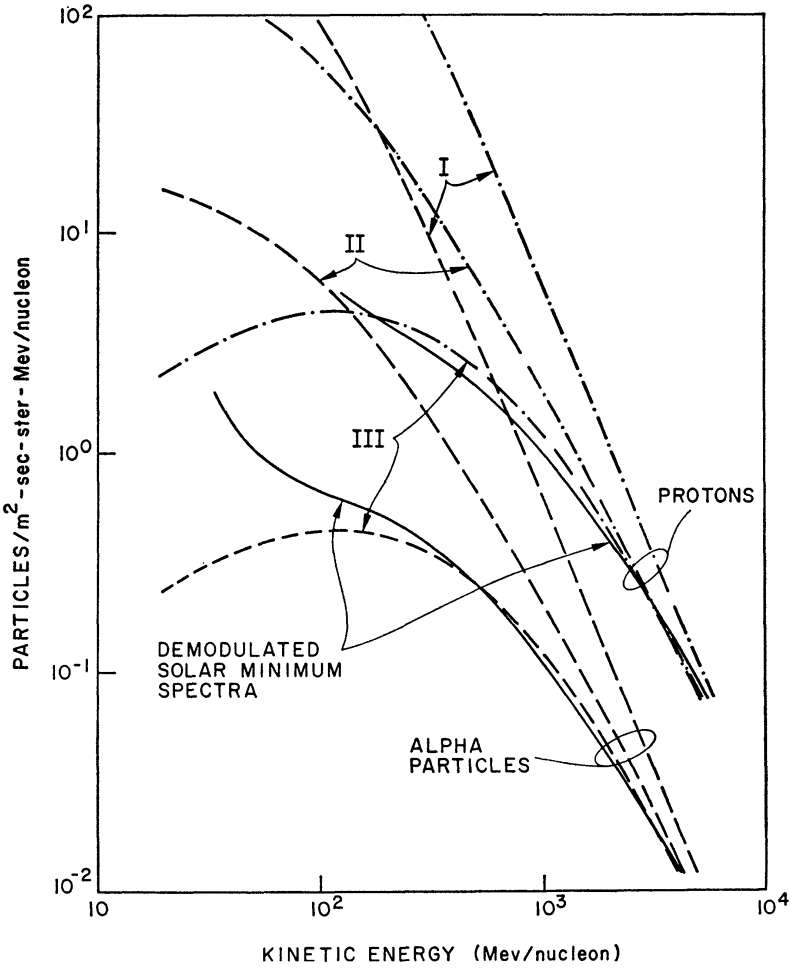


FIG. 15.—Interstellar equilibrium intensity of protons and alpha particles obtained by demodulating the observed solar-minimum spectra with the modulating function exp $(-0.35/R)$. Curves *I*, *II*, and *III* represent the equilibrium spectra which would result from homogeneously distributed cosmic-ray sources having energy spectra which are power laws in kinetic energy per nucleon, rigidity, and total energy per nucleon, respectively, for $x = 4$g cm$^{-2}$.

## REFERENCES

Badhwar, G. D., and Daniel, R. R. 1963, *Progr. Theoret. Phys.*, **30**, 615.
Badhwar, G. D., and Kaplon, M. F. 1966, *J. Geophys. Res.*, **71**, 5175.
Bailey, L. E. 1956, Reprint U.C.R.L.-3334, University of California Radiation Lab., Berkeley.
Balasubrahmanyan, V. K., Boldt, E., and Palmeira, R. A. R. 1967, *J. Geophys. Res.*, **72**, 27.
Balasubrahmanyan, V. K., Hagge, D. E., Ludwig, G. H., and McDonald, F. B. 1966*a*, *Proc. Internat. Conf Cosmic Rays, London*, **1**, 427.
———. 1966*b*, *J. Geophys. Res.*, **71**, 1771.
Baldoni, B., Focardi, S., Hromadnik, H., Monari, L., Saporetti, F., Femino, S., Mezzanares, F., Bertolini, E., and Gialanella, G. 1962, *Nuovo Cimento*, **26**, 1376.
Barkas, W. *Y.*, and Berger, M. J. 1964, NASA SP-3013.
Benveniste, J., and Cork, B. 1953, *Phys. Rev.*, **89**, 422.
Biswas, S., Lavakare, P. J., Ramadurai, S., and Sreenivasan, N. 1967, *Proc. Indian Acad. Sci.*, **65**, 104.

Biswas, S , Ramadurai, S., and Sreenivasan, N 1968, *Canadian J. Phys* , **46,** S593.
Brun, C., Leforth, M., and Tarrago, X. 1962, *J. Phys. Rad.*, **23,** 167.
Bunch, S. M., Forster, H. H., and Kim, C. C. 1964, *Nucl. Phys* , **53,** 241.
Cairns, D. J., Griffith, T. C., Lush, G J , Metheringham, A. J., and Thomas, R. H. 1964, *Nucl. Phys.*, **60,** 369.
Cameron, A. G. W. 1959, *Ap. J.*, **129,** 676.
Chapman, K. R., Jones, T. W., Khan, Q. H., McKee, J. S. C., Ray, H. B. van der, and Tanimura, Y. 1964, *Phys. Letters*, **11,** 253.
Comstock, G. M., Fan, C. Y., and Simpson, J. A. 1966, *Ap. J.*, **146,** 51.
Crawford, F. S., 1953, U.C.R.L. Rept. No. 1756, University of California Radiation Lab., Berkeley.
Currie, L. A. 1959, *Phys. Rev.*, **114,** 878.
Currie, L. A., Libby, W. F., and Wolfgang, R. L. 1956, *Phys. Rev.*, **101,** 1557.
Dahanayake, C., Kaplon, M. F., and Levakare, P. J. 1964, *J. Geophys. Res.*, **69,** 3681.
Davison, M., Hopkins, H. W. K., Lyons, L., and Shaw, D. F. 1963, *Phys. Letters*, **3,** 358.
Dennis, B. R., Badhwar, G. D., Deney, C. L., and Kaplon, M. F. 1967, *Bull. Am. Phys. Soc.*, **12,** 583.
Dorman, L. I. 1963, *Progress in Elem. Particle and Cosmic-Ray Phys.*, Vol. **7** (Amsterdam: North-Holland Publishing Co.), p. 1.
Durbin, B., Loar, H., and Steinberger, J. 1951, *Phys. Rev.*, **84,** 581.
Fan, C. Y., Gloeckler, G., Hsieh, K. C., and Simpson, J. A. 1966*a*, *Phys. Rev. Letters*, **16,** 813.
Fan, C. Y., Gloeckler, G., and Simpson, J. A. 1966*b*, *Phys. Rev. Letters*, **17,** 329.
Fichtel, C. E., and Reames, D. V. 1966, *Phys. Rev.*, **149,** 995.
Fickinger, W. J., Pickup, E., Robinson, D. K., and Salant, E. O. 1962, *Phys. Rev.*, **125,** 2082.
Fields, T. H., Fox, J. G., Kane, J. A., Stallwood, R. A., and Sutton, R. B. 1954, *Phys. Rev.*, **95,** 638.
Fireman, E. L., and Rowland, F. S. 1955, *Phys. Rev.*, **97,** 780.
Foster, F., and Mulvey, J. H. 1963, *Nuovo Cimento*, **27,** 93.
Freier, P. S., and Waddington, C. J. 1965, *J. Geophys. Res.*, **70,** 5753.
———. 1968, *ibid.*, **73,** 4261.
Gloeckler, G., and Jokipii, J. R. 1966, *Phys. Rev. Letters*, **17,** 203.
Guzhavin, V. M., Kliger, G. K., Kolganov, V. Z., Lebedev. A. V., Marish, K. S , Prokoshkin, Yu. D., Smolyankin, V. T., Sokolov, A. P., Soroko, L. M., and Wachuang, T. 1964, *Zh. Eksp. i Teor. Fiz.* **46,** 1245.
Hart, E. L., Louttit, R. I., Luers, D., Morris, T. W., Willis, W. J , and Yamamoto, S. S. 1962, *Phys. Rev.*, **126,** 747.
Hayakawa, S., Horikawa, N., Kajikawa, R., Kikuchi, K., Kobayakawa, H., Matsuda, K., Nagata, S., and Sumi, Y. 1964, *Phys. Letters*, **8,** 330.
Hayakawa, S., Ito, K., and Terashima, Y. 1958, *Progr. Theoret. Phys., Suppl.*, **6,** 1.
Hofmann, D. J., and Winckler, J. R. 1966, *Phys. Rev. Letters*, **16,** 109.
Honda, M., and Lal, D. 1960, *Phys. Rev.*, **118,** 1618.
Innes, W. H. 1957, U.C.R.L. Rept. No. 8040, University of California Radiation Lab., Berkeley.
Jokipii, J. R. 1966, *Ap. J.*, **146,** 480.
———. 1968, *Canadian J. Phys.*, **46,** S950.
Jokipii, J. R., and Coleman, P. J. 1968, *J. Geophys. Res.*, **73,** 549.
Kavaloski, C. D., Bassani, G., and Hintz, N. M. 1963, *Phys. Rev.*, **132,** 813.
Kozadaev, M. S., Kulyukin, M. M., Sulyaev, R. M., Filippov, A. I., Shcherbakov, Yu A. 1960, *Zh. Eksp. i Teoret. Fiz.*, **38,** 708.
Kuzhevskii, B. M. 1966, *Yader. Fiz.*, **4,** 130.
Legg, J. C. 1963, *Phys. Rev.*, **129,** 272.
Meyer, J. P., Hagge, D. E., and McDonald, F. B. 1968, *Canadian J. Phys.*, **46,** S503.
Moulthrop, P. H. 1955, *Phys. Rev.*, **99,** 1509.
Nadi, M., and Riad, F. 1964, *Nucl. Phys.*, **50,** 33.
Neganov, B. S., and Parfenov, L. B. 1958, *Zh. Eksp. i Teoret. Fiz.*, **34,** 767.
O'Dell, F. W., Shapiro, N. M., Silberberg, R., and Stiller, B. 1966, *Proc. Internat. Conf Cosmic Rays, London*, **1,** 412.
Oers, W. T. H. van. 1963, unpublished Ph.D., thesis. University of Amsterdam.
O'Gallagher, J. 1967, *Ap. J.*, **150,** 675.
O'Gallagher, J., and Simpson, J. A. 1967, *Ap. J.*, **147,** 819.
Ormes, J. F., and Webber, W. R. 1966, *Proc. Internat. Conf. Cosmic Rays, London*, **1,** 349.
Parker, E. N. 1958, *Phys. Rev.*, **110,** 1445.
Pickup, E., Robinson, D. K., and Salant, E. O. 1962, *Phys. Rev.*, **125,** 2091.
Ramaty, R., and Lingenfelter, R. E. 1968, *Canadian J. Phys.*, **46,** S627.
Riddiford, L., and Williams, A. W. 1960, *Proc. Roy. Soc. London, A*, **257,** 316.
Rosenfeld, A. H. 1954, *Phys. Rev.*, **96,** 139.
Schulz, A. H. 1952, U.C.R.L. Rept. No. 1756, University of California Radiation Lab , Berkeley.
Schwarzschild, A., and Zupancic, C. 1963, *Phys. Rev.*, **129,** 854.
Selove, W., and Teem, J. M. 1958, *Phys. Rev.*, **112,** 1658.

Shapiro, M. M., and Silberberg, R. 1968, *Canadian J. Phys* , **46**, S561.
Smith, G. A., Courant, A. H., Fowler, E. C., Kraybill, H., Sandweiss, J., and Taft, H. 1961, *Phys. Rev.*, **123**, 2160.
Smith, W. R., and Ivash, E. V. 1962, *Phys. Rev.*, **128**, 1175.
Stadler, H. L. 1954, *Phys. Rev.*, **96**, 496.
Stevenson, M. L. 1953, U.C.R.L. Rept. No. 2188, University of California Radiation Lab., Berkeley.
Suess, H. E., and Urey, H. C. 1956, *Rev. Mod. Phys.*, **28**, 53.
Tannenwald, P. O. 1953, *Phys. Rev.*, **89**, 508.
Waddington, C. J., and Freier, P. S. 1966, *Proc. Internat. Conf. Cosmic Rays, London*, **1**, 345.
Wickersham, A. F. 1957, *Phys. Rev.*, **107**, 1050.